IEEE Access
Multidisciplinary ⋮ Rapid Review ⋮ Open Access Journal

Received November 9, 2020, accepted December 10, 2020, date of publication December 17, 2020,
date of current version December 30, 2020.

Digital Object Identifier 10.1109/ACCESS.2020.3045416

Disturbance Observer-Based Linear Matrix Inequality for the Synchronization of Takagi-Sugeno Fuzzy Chaotic Systems

VAN NAM GIAP[1], SHYH-CHOUR HUANG[1], (Senior Member, IEEE), QUANG DICH NGUYEN[2], AND TE-JEN SU[3,4], (Senior Member, IEEE)

[1]Department of Mechanical Engineering, National Kaohsiung University of Science and Technology, Kaohsiung 807618, Taiwan, R.O.C.
[2]Institute for Control Engineering and Automation, Hanoi University of Science and Technology, Hanoi 100000, Vietnam
[3]Department of Electronic Engineering, National Kaohsiung University of Science and Technology, Kaohsiung 807618, Taiwan, R.O.C.
[4]Graduate Institute of Clinical Medicine, Kaohsiung Medical University, Kaohsiung 807378, Taiwan, R.O.C.

Corresponding author: Shyh-Chour Huang (shuang@nkust.edu.tw)

This work was supported by the Ministry of Science and Technology, Republic of China, under Contract MOST 109-2622-E-992-008-CC3.

ABSTRACT This article presents a synchronization control method based on poles' placement, disturbances, and uncertainty estimation (DUE) for a pair of Takagi-Sugeno fuzzy systems. First, a 3-D chaotic system was completely converted into a Takagi-Sugeno (T-S) fuzzy model by applying the nonlinearity sector method, which consists of if-then rules and sub-linear systems. Second, two identical T-S fuzzy systems with different initial conditions were synchronized by applying the linear matrix inequality (LMI) to place the eigenvalues of the state error equations in the stable region. Third, the sum of the time-varying disturbances and uncertainties of two nonidentical T-S fuzzy systems were deleted by a disturbance and uncertainty estimation. The given output signals confirmed that the proposed method is suitable and ideal for synchronizing T-S fuzzy systems. The ideas of control theory were implemented by using two experimental scenarios in MATLAB Simulink for two computers connected via an internet router and an electronics circuit's communication.

INDEX TERMS Disturbance and uncertainty estimation, linear matrix inequality, synchronization, T-S fuzzy systems.

I. INTRODUCTION

In recent years, industrial production has been rapidly growing to adapt to the 4.0 industry revolution's requirements, and the database is one of the most important keys to the success of this revolution. Following the development of data transmission techniques, the security of the data is critical. However, the data are not just transmitted as a box of data; sometimes, the data need online transmission, and because of this requirement, the synchronization of transmission communication is a potential job for many engineers and scientists. Data-secure communications also offer potential jobs, as the secure communication of a data transmission based on a chaotic system is a reality. Chaotic systems influence secure communications and information science due to the potential of the chaotic system to be unpredictable, sensitive to the initial conditions, and nonperiodic [1]. Huang *et al.* [2] presented the applications and the synchronization method of 4-D chaotic systems with an application to image encryption. Mobayen and Tchier [3] proposed a synchronization for the chaotic system with Lipschitz nonlinearity by using a linear matrix inequality. The synchronization of network systems appeared in [4]–[9]. The field of data science with encrypted images also has many papers that deal with chaotic systems. Liu *et al.* [10] proposed the method of image encryption using complex hyper-chaotic systems by injecting the impulse parameter method. Wang *et al.* [11] used a chaotic map to encrypt an image on the bit level. Yang *et al.* used the fractional order chaotic system to achieve color image compression [12]. The application of chaotic system synchronization to the electronics circuit has been revealed in [13]–[16]. The synchronization of the chaotic system application of computer-to-computer communications via internet devices was presented by Chen *et al.* [17]. Their paper proposed the synchronization methodology for the multiscroll Chen chaotic system based on computer

The associate editor coordinating the review of this manuscript and approving it for publication was Wei Xu.

communication via a local network. With the motivation of these previously published papers, this article discusses the synchronization of the chaotic system based on the Takagi-Sugeno fuzzy model, which has had minimal investigation. Furthermore, disturbance and uncertainty are complications of the chaotic system, and they were deleted mostly by applying the time-varying disturbance observer in this article.

The Takagi-Sugeno fuzzy modeling method was revealed in 1985 [18]. The method plays the role of a nonlinear system in mathematical modeling by if-then fuzzy rules and sublinear systems. Due to the rapid development of computer speed, the T-S method has been studied by many papers [19]–[27]. To take advantage of the T-S fuzzy system, the synchronization of the chaotic system has been reconstructed in the form of a T-S system [28]–[33]. To the best of the author's knowledge, there are few synchronizations of two nonidentical systems that use the T-S fuzzy system with the disturbance observer, and the implementation of this complication on the real system has not been executed. Lendek *et al.* [34] presented the methodology of constructing the T-S fuzzy system, and there are a few options, such as sector nonlinearity and linearization. This study used sector nonlinearity to convert a 3-D fan-shaped chaotic system into a T-S fuzzy model, where the 3-D chaotic system was proposed by Liu *et al.* [35]. The advantages of the 3-D chaotic system are difficult to realize in secure encrypted signals, and they are sensitive to disturbances in the constant term. However, the constant term in the range of existence will maintain the system phase portraits in the chaotic maps, as paper [35] shows. The disadvantage of the constant term is that it is easily affected by disturbance. When a disturbance in the third state of the system cannot be cancelled completely, the third state will be changed greatly, which the reason to use a disturbance and uncertainty observer. Due to the form of the chaotic system, the disturbance and system parameter variation are difficult to calculate directly. The form of the T-S fuzzy system could render it easier to interfere with these terms. The disturbance and uncertainty rejection impact control theory, which causes the system to be more stable. In the nonlinear disturbance observer proposed by Chen [36], the time derivative of the disturbance is assumed to be equal to zero. In fact, whereas the first derivative of a disturbance with a low frequency goes to zero, this behavior does not occur with a high-frequency disturbance. This distinction motivated us to propose the new mathematical mode of a disturbance observer for both low and high frequencies. The model of the disturbance observer is based on input control and output response signals. To stabilize the master and slave systems of the communication, the control algorithm should be perfectly designed. This study took advantage of the linear matrix inequality that was proposed by Chilali *et al.* [37] and Mahmoud and Pascal [38] to design the controller, which applied the *D*-stability to seek feedback gains when the eigenvalues of the system can be found in perfect locations with a small rise time, small overshoot, small damping ratio, etc. For computer-secure communications, the gains are not limited; however, for electronic circuits, the gains need to be small to be suitable for electronic components' functions.

In previously published papers [3], [9], and [32], the overshoots and settling times of the tracking error values between master and slave systems in simulations of these proposed methods were still high and large, respectively. In [3], the control method is simple, which leads to larger synchronization-error rise times and overshooting than our paper. These papers dealt with continuous-bounded functions to cope with disturbances and uncertainty, with the assumptions of a time-varying function and a stratified Lipschitz function. Paper [9] proposed the synchronization control and application for an industrial internet of things, where the Lyapunov stability has been applied to design the control synchronization. However, this article did not investigate disturbances and uncertainty rejections, and the conjunctions of real experimental conditions were ignored. In [32], the Bessel–Legendre Inequality method was applied to synchronize the coronary artery state time-delay system, which was a simple structure with a good outcome. However, the paper ignored the disturbance and uncertainty that exist in real applications. To resolve the limitations of the previous paper, this article addresses problems that the prior paper did not investigate, which can be considered as the advantage of this study. The high-frequency disturbances and uncertainties were all deleted by the new disturbance observer and D-stability with an air gap. The main contributions of this paper are as follows:

1) A three-dimensional chaotic system with a fan shape has been analyzed in detail by constructing the T-S fuzzy model.
2) The linear matrix inequality with D-stability has been applied to determine the stable region of the error states' eigenvectors, which was solved by convex optimization.
3) Fast-varying disturbance terms were cancelled by applying a new disturbance and uncertainty estimator, and the convergence of the proposed disturbance observer was proven completely.
4) The experiments of two cases have been executed perfectly, and they consist of two computer communication systems with the use of MATLAB and electronic circuits' communication.

The organization of the paper is as follows: Section I gives a brief introduction to the system and the trends of research. Section II presents the problem formulations and system mathematical models. Section III describes the synchronization control method and the disturbance and uncertainty estimator concepts. Then, Section IV gives an illustrative example study. Finally, Section V provides the conclusion.

Notations: The signs of $A > 0$ and $A < 0$ indicate positive and negative matrices, respectively. I is the identity matrix, and A^T is the transposed matrix of A. In addition, A^{-1} is the inverse matrix of A.$R^{m\times n}$ is defined as a matrix with m lines and n rows. $n_0^1(\cdot)$ and $n_1^1(\cdot)$ are the outer membership functions of the fuzzy system.

II. MATHEMATICAL MODELLING AND PROBLEM FORMULATION

Previously, the three-dimensional fan shape system of [35] was given as.

$$\begin{cases} \dot{x}(t) = -ax(t) + by(t) \\ \dot{y}(t) = -x(t)z(t) \\ \dot{z}(t) = cx^2(t) + x(t)y(t) - d \end{cases} \tag{1}$$

Alternatively, the system in Eq. (1) can be transferred to other forms as follows:

$$\begin{bmatrix} \dot{x}(t) \\ \dot{y}(t) \\ \dot{z}(t) \end{bmatrix} = \begin{bmatrix} -a & b & 0 \\ 0 & 0 & -x(t) \\ cx(t) & x(t) & 0 \end{bmatrix} \begin{bmatrix} x(t) \\ y(t) \\ z(t) \end{bmatrix} + \begin{bmatrix} 0 \\ 0 \\ -1 \end{bmatrix} d \tag{2}$$

The term d in system (1) is sensitive to disturbance and uncertainty values; therefore, the disturbance and uncertainty estimation has been directly constructed, and it is understood that the term d is an unexpected term. The value of d determines the phase portrait behaviors of the system. The parameters of the system are now determined as $a = 1$, $b = 2$, $c = 1$, and $d = 3$. Therefore, the disturbance and uncertainty rejection play important roles. In fact, the disturbance observer for system (1) is difficult to complete. Because of this weak point, system (1) could be represented by a T-S fuzzy model, which is achieved by applying the nonlinearity sector method to obtain the system model in the fuzzy rules and linear subsystems. A sector nonlinearity was applied to change the system states' equation from Eq. (1) to the T-S fuzzy model. The method considered the system as the following equation:

$$\begin{cases} \dot{X}(t) = f^m(x(t), u(t))X(t) + g^m(x(t), u(t))u(t) + Dd(t) \\ Y(t) = h(x(t), u(t))X(t) \end{cases} \tag{3}$$

where f^m, g^m and h^m are smooth functions, with the assumption that the disturbance $Dd(t)$ is bounded. The scheduling variables are selected as $x_j(\cdot) \in [\min_l, \max_l]$, and the weighting functions are determined as follows:

$$\begin{cases} n_0^l(\cdot) = \dfrac{\max_l - x_l(\cdot)}{\max_l - \min_l} \\ n_1^l(\cdot) = 1 - n_0^l(\cdot) \end{cases} \tag{4}$$

The functions $n_0^l(\cdot)$ and $n_1^l(\cdot)$ are positively defined, and these values satisfy $n_1^l(\cdot) + n_0^l(\cdot) = 1$. Here, $[\min_l, \max_l]$ is the domain of $x_j(\cdot)$. Generally, the T-S fuzzy model can be understood as the following equation:

$$\begin{cases} \delta X(t) = \sum_{i=1}^{r} \omega_i(\theta(t))\{(A_iX(t) + \Delta A_iX(t)) \\ \qquad + (B_iu(t) + \Delta B_iu(t)) + D_id(t)\} \\ Y(\tau) = CX(t) \end{cases} \tag{5}$$

where $\delta X(t)$ denotes the derivative $\dot{X}(t)$, and t can be used to represent the continuous time. $X(t) \in R^{n\times q}$, $u(t) \in R^{m\times q}$, and $Y(t) \in R^{p\times q}$ are the system states, control input, and output vectors, respectively. Furthermore, $d(t) \in R^{k\times q}$ is the disturbance, and it consists of outside disturbance. $A_i \in R^{n\times n}$, $B_i \in R^{n\times m}$, and $C_i \in R^{p\times n}$ are the state matrix, input matrix and output matrix, respectively. $\Delta A_i \in R^{n\times n}$ and $\Delta B_i \in R^{n\times m}$ are unknown dynamic terms of matrices A and B, respectively. $D_i \in R^{n\times k}$ is the matrix of the disturbance term.

The weight $\sum_{i=1}^{r} \omega_i(\theta(t)) = 1$. System (5) can be modified as in the following equation:

$$\begin{cases} \delta X(t) = \sum_{i=1}^{r} \omega_i(\theta(t))\{(A_iX(t)) + (B_iu(t)) + E_iL(t)\} \\ Y(t) = CX(t) \end{cases} \tag{6}$$

where $E_iL(t) = \Delta A_iX(t)) + \Delta B_iu(t) + D_id(t)$ is the term of the uncertainty value. The first state is assumed belong to $x(t) \in [-\gamma; \gamma]$, and the lumped uncertainty$E_iL(t) < L_1$. Applying the sector nonlinearity to system (2) yields $\omega_1(\theta(t)) = \frac{\gamma + x(t)}{2\gamma}$ and $\omega_2(\theta(t)) = \frac{\gamma - x(t)}{2\gamma}$.

$$A_1 = \begin{bmatrix} -1 & 2 & 0 \\ 0 & 0 & -\gamma \\ \gamma & \gamma & 0 \end{bmatrix}, \quad B_1 = \begin{bmatrix} 0 \\ 1 \\ 1 \end{bmatrix}, \quad E_1 = \begin{bmatrix} 1 \\ 1 \\ 1 \end{bmatrix},$$

$$A_2 = \begin{bmatrix} -1 & 2 & 0 \\ 0 & 0 & \gamma \\ -\gamma & -\gamma & 0 \end{bmatrix}, \quad B_2 = \begin{bmatrix} 0 \\ 1 \\ 1 \end{bmatrix}, \quad E_2 = \begin{bmatrix} 1 \\ 1 \\ 1 \end{bmatrix} \text{ and}$$

$$C = [\,1 \quad 0 \quad 0\,].$$

Since we have this potential, the synchronization of paired T-S fuzzy models with different initial conditions were applied. The system states of Eq. (6) are achieved by MATLAB simulations, as shown in Fig. (1) below.

In Fig. 1, the system state in the first 100 seconds is shown with no periodic and chaotic trajectories. The system phase portraits are shown in Fig. 2 below.

Two experiments have been performed, and the system on the electronics circuit could be converted by the amplifier and multiple components' characteristics. Whenever the derivative of the system can be represented by the capacitor, the multiple system state can be converted by multiple devices. In this section, the systems' mathematical model in an electronic circuit will be discussed; this model was obtained from the OrCAD Capture software. The time scale of the system was reduced 1000 times by reducing the resistance values, which are linked to capacitors c1, c2, and c3. The time scale reduction is intended to achieve better signal compression in the higher frequency. This conversion can preserve all of the original system's characteristics. The time scaling affects the selection of, e.g., the electronic components and the signal encryption frequency. Furthermore, the phase portrait of the system is still mostly the same as the MATLAB simulation. All of the details of the T-S fuzzy system in Eq. (6) are shown in the following Appendix and Fig. 1. The three-dimensional Takagi-Sugeno system in Eq. (6) has been implemented in the electronic circuit simulation.

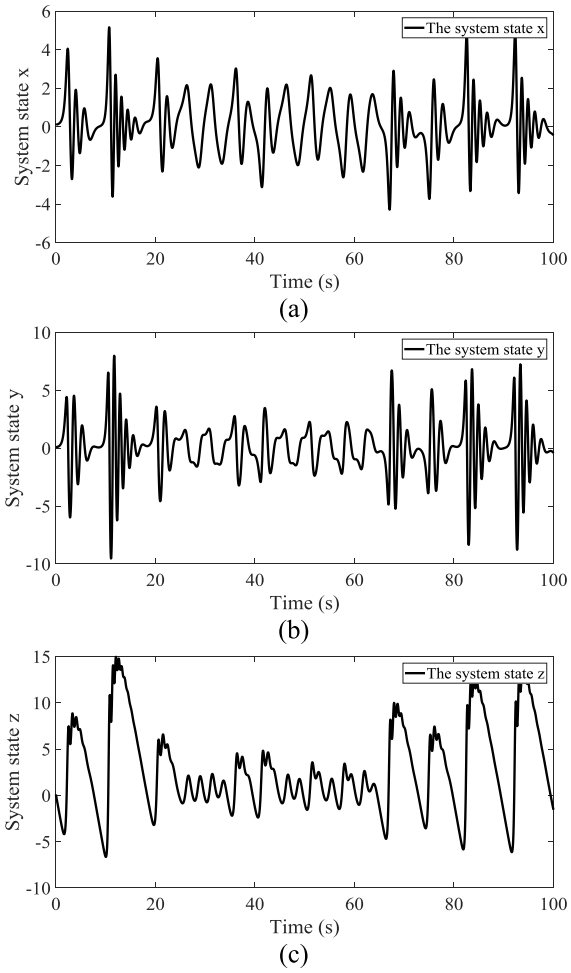

FIGURE 1. System behaviors with respect to the initial conditions $x(0) = 0.1$, $y(0) = 0.1$, $z(0) = 0.1$, and $x(t) \in [-5; 5]$: (a) x-axis trajectory, (b) y-axis trajectory, (c) z-axis trajectory.

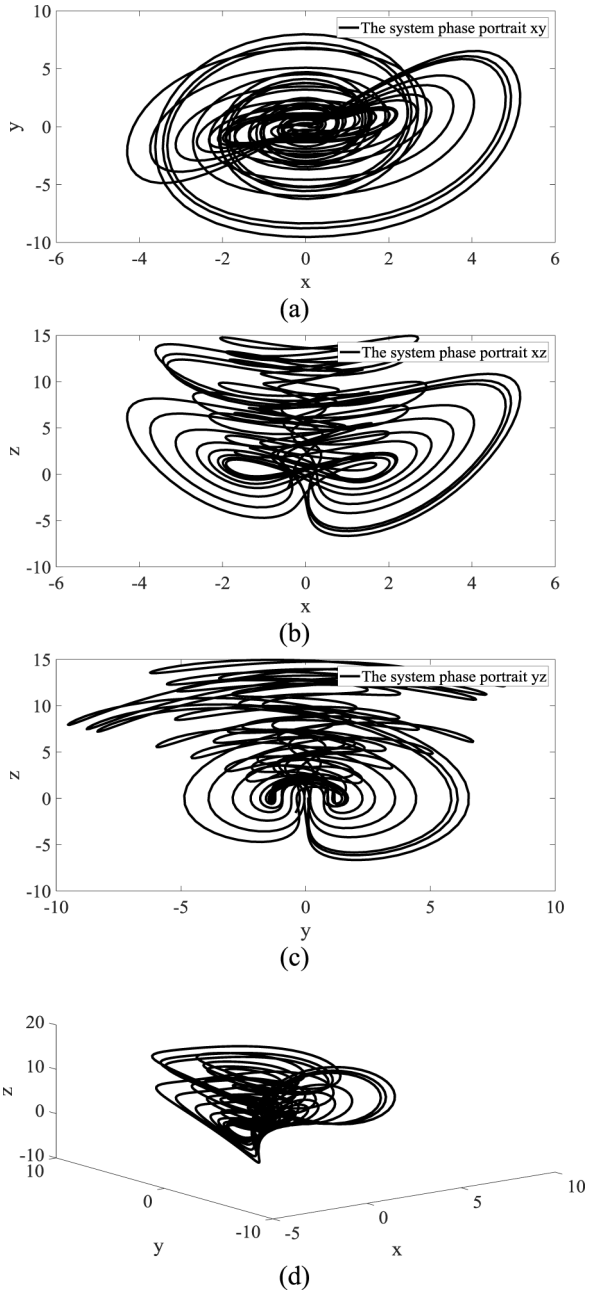

FIGURE 2. System phase portraits in two axis coordinates and three coordinates with respect to the initial conditions $x(0) = 0.1$, $y(0) = 0.1$, $z(0) = 0.1$, and $x(t) \in [-5; 5]$: (a) y-x phase portrait, (b) z-x phase portrait, (c) z-y phase portrait, (d) x-y-z phase portrait.

The x-, y-, and z-axes reveal the general chaotic states. The system phase portraits are shown in Figure 3.

The system states are shown in Figure 4 below.

The system trajectories will differ due to application of different conditions; however, the phase portrait shapes are similar due to the system characteristics. To synchronize two nonidentical T-S fuzzy systems, the control synchronization and disturbance observer need to be perfectly constructed for the system. This study proposes the disturbance observer based linear matrix inequality to achieve the desired performances. For clarity, the system states of Eq. (1) can be used as $x \rightarrow x_{m1}$ or $x \rightarrow x_{s1}$, $y \rightarrow x_{m2}$, or $y \rightarrow x_{s2}$, and $z \rightarrow x_{s3}$, or $x \rightarrow x_{s1}$ for the master and slave states, respectively.

III. DISTURBANCE OBSERVER-BASED LINEAR MATRIX INEQUALITY FOR SYNCHRONIZATION OF THE TAKAGI-SUGENO FUZZY CHAOTIC SYSTEM

This study reused the mathematical mode of paper [35] to build a new T-S fuzzy mode, as shown in Eq. (6). The master and slave system are now defined as follows:

$$\begin{cases} \dot{x}_{1m}(t) = -(a + \Delta a)x_{m1}(t) + (b + \Delta b)x_{m2}(t) + d_{m1}(t) \\ \dot{x}_{2m}(t) = -x_{1m}(t)x_{3m}(t) + d_{m2}(t) \\ \dot{x}_{3m}(t) = (c + \Delta c)x_{1m}^2(t) + x_{m1}(t)x_{m2}(t) - d + d_{m3}(t) \end{cases} \tag{7}$$

where x_{im} are the master system states with the known values a, b, c, and d. In additional, we have the unknown system parameters Δa, Δb, and Δc as variations of the terms a, b,

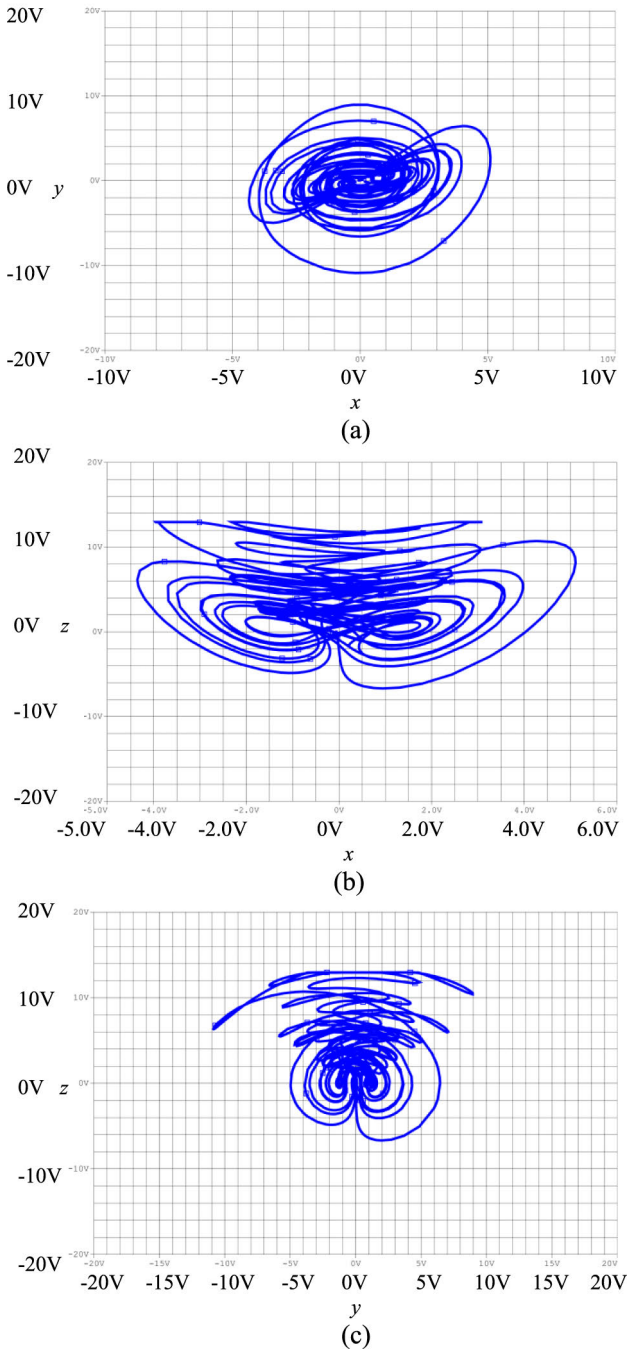

FIGURE 3. System phase portraits on the micro second scale: (a) y-x phase portrait, (b) z-x phase portrait, (c) z-y phase portrait.

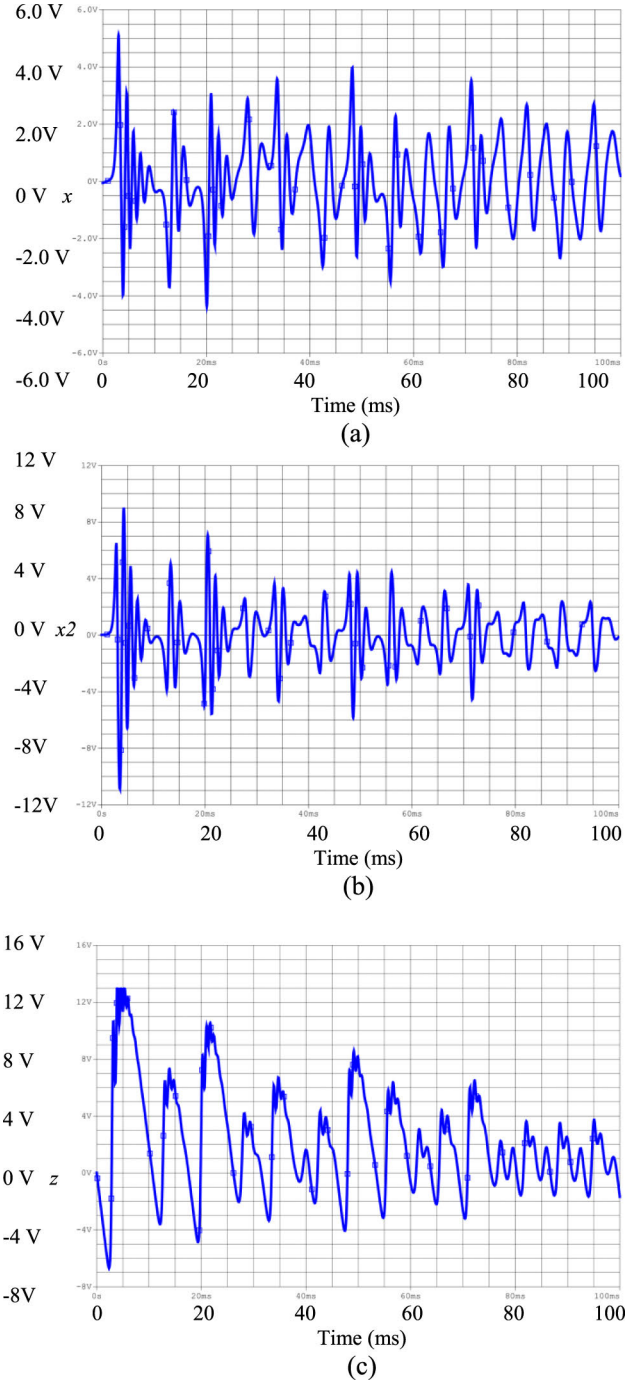

FIGURE 4. System states on the micro second scale: (a) x-axis, (b) y-axis, (c) z-axis.

and c, respectively. Furthermore, $d_i(\mathrm{t})$ are the disturbances of x_{im} for $i = 1 \div 3$. The slave system is defined in the following equation:

$$\begin{cases} \dot{x}_{1s}(\mathrm{t}) = -(a+\Delta a)x_{s1}(\mathrm{t}) + (b+\Delta b)x_{s2}(\mathrm{t}) + d_{s1}(\mathrm{t}) \\ \dot{x}_{2s}(\mathrm{t}) = -x_{1s}(\mathrm{t})x_{3s}(\mathrm{t}) + d_{s2}(\mathrm{t}) + u_1(\mathrm{t}) \\ \dot{x}_{3s}(\mathrm{t}) = (c+\Delta c)x_{1s}^2(\mathrm{t}) + x_{s1}(\mathrm{t})x_{s2}(\mathrm{t}) - d + d_{s3}(\mathrm{t}) \\ \qquad\qquad + u_2(\mathrm{t}) \end{cases} \tag{8}$$

where the term m is represented as the slave. After applying sector nonlinearity for both the master and slave systems, the master system is now defined as follows:

$$\begin{cases} \delta X_m(\mathrm{t}) = \sum_{i=1}^{r} \omega_{mi}(x_{1m}(\mathrm{t}))\{(A_i X_m(\mathrm{t})) + G_i d + E_{im} L_m(\mathrm{t})\} \\ Y_m(\mathrm{t}) = C X_m(\mathrm{t}) \end{cases} \tag{9}$$

where $E_{im}L_m(t) = \Delta A_i X_m(t)) + D_i d_{mi}(t)$ is the lumped uncertainty and disturbance of the master system. We assume that the lumped disturbance and uncertainty is bounded such that $E_{im}L_m(t) < l_m$, where l_m is an unknown constant value. $G_i = [0\ 0\ -1]^T$ and d are the constant terms. The slave system is defined as

$$\begin{cases} \delta X_s(t) = \sum_{i=1}^{r} \omega_{si}(x_{1s}(t))\{A_i X_s(t) + B_i u(t) + G_i d(t) \\ E_{is}L_s(t)\} \\ Y_s(t) = CX_s(t) \end{cases} \tag{10}$$

where $E_{is}L_s(t) = \Delta A_i X_s(t)) + \Delta B_i u(t)) + D_i d_{si}(t)$ is the lumped disturbance and uncertainty of the slave system. The lumped uncertainty is assumed to be $E_{is}L_s(t) < l_s$, where l_s is an unknown constant value. The error of the system is defined as $e(t) = X_m(t) - X_s(t)$, where

$$e(t) = X_m(t) - X_s(t) = \begin{bmatrix} x_{1m}(t) - x_{1s}(t) \\ x_{2m}(t) - x_{2s}(t) \\ x_{2m}(t) - x_{2s}(t) \end{bmatrix} \tag{11}$$

To construct the controller for synchronizing the master and slave system, this study proposed the linear matrix inequality-based poles placement with D-stability. The uncertainty and disturbance were suppressed by a fast-varying disturbance observer. For more detail, the linear matrix inequality was used. This inequality is briefly described.

A. LINEAR MATRIX INEQUALITY-BASED POLES PLACEMENT

Basically, the states feedback and output feedback are simple and effective control methods. These control methods are simple and easy to implement in both hardware and software. The system eigenvalues are determined in the stable region of the complexity plane. The linear matrix inequality is usually used to determine the system eigenvalues, which should be located in the left-half plane. The region of the poles defines both the transient response speed and the gain magnitude of the controller. Generally, the system poles are stable when the eigenvector of the system state matrix is represented as $\lambda_i = -a_i \pm b_i j$, where a_i and b_i are positively defined. The factors of the damping ratio, damped nature frequency, rise time, and settling time are related to the eigenvalues' locations. For the continuous time, the poles should be located in the left-half of the complexity plane. There were many methods for determining the control gain, but this study applied the pole placement method based on the conic region. The $\dot{x}(t) = Ax(t)$ is called D-stable when the system poles are located in region D [35]–[37]. A is stable when the symmetric condition with P is satisfied:

$$AP + PA^T < 0, \quad P > 0 \tag{12}$$

A subset D is called LMI if there exists a symmetric matrix $a = a_{kl} \in R^{m\times m}$, $b = b_{kl} \in R^{m\times m}$ and

$$D = (z \in C : \quad f_D < 0) \tag{13}$$

where

$$f_D = a + zb + \bar{z}b^T = a_{kl} + b_{lk}z + b_{lk}\bar{z} \tag{14}$$

with $1 \le k, l \le m$. For the disk region, (c,r) is shown in Figure. 5 below.

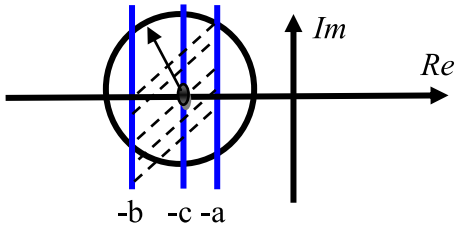

FIGURE 5. LMI in region D.

This article applied the LMI poles placement of [39], where the D region is determined as follows:

$$D_{rc} = \{z \in C | ((z + c)(\bar{z} + c) - r^2 < 0\} \tag{15}$$

where r and c are the radius and center of the disk region, respectively. The characteristic of Eq. (15) can be rewritten as follows:

$$\begin{aligned} F_{D_{rc}} &= \begin{bmatrix} -r & c + z \\ c + \bar{z} & -r \end{bmatrix} \\ &= Q + zW + \bar{z}W^T \end{aligned} \tag{16}$$

where the matrix $Q = \begin{bmatrix} -r & q \\ q & -r \end{bmatrix}$ and $W = \begin{bmatrix} 0 & 1 \\ 0 & 0 \end{bmatrix}$. The transient response, damping ratio, and overshoot are all dependent on the location of the system eigenvalue, which are determined as the eigenvalue of the matrix A of the system $\dot{x}(t) = Ax(t)$. To design the system, the eigenvalue will be located in $-b < Re(\det(A)) < -a$ if the following equation is satisfied.

$$\begin{cases} (A + aI)P + P(A + aI)^T < 0 \\ (A + bI)P + P(A + bI)^T > 0 \end{cases} \tag{17}$$

or

$$\begin{cases} AP + PA^T + 2aP < 0 \\ AP + PA^T + 2bP > 0 \end{cases} \tag{18}$$

where a and b are positively defined. The stability in Eq. (18) can be defined as

$$\begin{bmatrix} -rP & cP + PA^T \\ cP + PA & -rP \end{bmatrix} < 0 \tag{19}$$

Proof: This section generally proved the convergence of the linear matrix inequality. We define the Lyapunov condition candidate as follows:

$$V(t) = x^T(t)Px(t) \tag{20}$$

Taking the derivative of Eq. (20) leads to

$$\begin{aligned} \dot{V}(t) &= \dot{x}^T(t)Px(t) + x^T(t)P\dot{x}(t) \\ &= (Ax(t))^T Px(t) + x^T(t)PAx(t) \\ &= x^T(t)A^T Px(t) + x^T(t)PAx(t) \end{aligned} \tag{21}$$

The Lyapunov condition is satisfied when $AP+PA^T < 0$. The proof is completed for the basic state feedback by applying the linear matrix inequality; this concept will appear in the next section.

This section briefly reintroduces the D-stability. Here, we give more details of the D-stability with a predetermined air gap.

The advantages of the D-stability are as follows:

- D-stability is an easily implemented condition for the control design, which obtains the system eigenvalues directly by using the optimization method.

- The damping, overshooting, settling time, rise time, and damped nature are all easily and effectively achieved by applying the D-stability.

- In a comparison of the D-stability to the Lyapunov condition, the controller gains of applying the D-stability are easier than for the Lyapunov condition.

- The D-stability is a subset of the $\alpha-$stability, where the control system eigenvalues of the D-stability could be obtained in a specific area.

B. TIME-VARYING DISTURBANCE OBSERVER

Consider the system

$$\dot{X}(t) = G_1X(t) + G_2u(t) + G_3d(t) \tag{22}$$

where $X(t) \in R^{m\times n}$ are the system states, $u(t) \in R^{p\times n}$ is the control input, and $d \in R^{q\times n}$ is the disturbance of the system. $G_1 \in R^{m\times m}$, $G_2 \in R^{m\times p}$, $G_3 \in R^{m\times q}$ are the approximated matrix of the states, control input, and disturbance, respectively. The traditional nonlinear disturbance observer proposed by Chen [36] can be represented as

$$\begin{cases} \dot{p}(t) = -L_dG_3p(t) - L_d(G_1X(t) + G_2u(t) + G_3q(t)) \\ q(t) = L_dX(t) \\ \hat{d}(t) = p(t) + q(t) \end{cases} \tag{23}$$

where $L_d \in R^{q\times m}$ is the disturbance observer gain, $p(t) \in R^{q\times n}$ is the disturbance state vector, $q(t) \in R^{q\times n}$ is an auxiliary vector of disturbance states, and $\hat{d}(t) \in R^{q\times n}$ is the observed disturbance. Taking the derivative of the estimated disturbance yields

$$\begin{aligned} \dot{\hat{d}}(t) &= \dot{p}(t) + \dot{q}(t) \\ &= -L_dG_3p(t) - L_d(G_1X(t) + G_2u(t) \\ &\quad + G_3q(t)) + L_d\dot{X}(t) \\ &= -L_dG_3p(t) - L_d(G_1X(t) + G_2u(t) \\ &\quad + G_3q(t)) + L_d(G_1X(t) + G_2u(t) + G_3d(t)) \\ &= -L_dG_3(p(t) + q(t)) + L_dG_3d(t) \\ &= L_dG_3\tilde{d}(t) \end{aligned} \tag{24}$$

Subtracting the derivative of the disturbance on both sides of Eq. (24) leads to

$$\dot{d}(t) - \dot{\hat{d}}(t) = \dot{d}(t) - L_dG_3\tilde{d}(t) \tag{25}$$

or

$$\dot{\tilde{d}}(t) = \dot{d}(t) - L_dG_3\tilde{d}(t) \tag{26}$$

Here, $\tilde{d}(t) = d(t) - \hat{d}(t)$ is referred to as the disturbance error value. For a disturbance error converging to zero when time goes to infinity, this nonlinear disturbance observer requires that the disturbance varies slowly or its derivative $\dot{d}(t) = 0$. Due to this disadvantage, this study is proposing a new method to suppress the term of disturbance with a fast-varying disturbance mixed with uncertainty. The new observer is now introduced as

$$\begin{cases} \dot{p}(t) = -L_dG_3p(t) - L_d(G_1X(t) + G_2u(t) + G_3q(t)) \\ q(t) = L_dX(t) \\ \hat{d}_{new}(t) = (\alpha + 1)(p(t) + q(t)) + \beta(\dot{p}(t) + \dot{q}(t)) \end{cases} \tag{27}$$

where α and β are positive values and are chosen conditionally such that $\alpha/\beta > 1.\hat{d}(t)$ is subset of $\hat{d}_{new}(t)$. The initial disturbance states are $p(0) = 0$ and $q(0) = 0$. The convergence of the disturbance observer is proved to be

$$\dot{\hat{d}}_{new}(t) = (\alpha + 1)(\dot{p}(t) + \dot{q}(t)) + \beta(\ddot{p}(t) + \ddot{q}(t)) \tag{28}$$

Subtracting the derivative of the disturbance from both sides of Eq. (25) yields

$$\begin{aligned} \dot{\tilde{d}}_{new}(t) &= \dot{d}(t) - [(\alpha + 1)(\dot{p}(t) + \dot{q}(t)) + \beta(\ddot{p}(t) + \ddot{q}(t))] \\ &= \dot{d}(t) - \dot{\hat{d}}(t) - [(\alpha)(\dot{p}(t) + \dot{q}(t)) + \beta(\ddot{p}(t) + \ddot{q}(t))] \\ &= \dot{\tilde{d}}(t) - [(\alpha)(\dot{p}(t) + \dot{q}(t)) + \beta(\ddot{p}(t) + \ddot{q}(t))] \end{aligned} \tag{29}$$

where $\dot{\tilde{d}}_{new}(t) = \dot{d}(t) - \dot{\hat{d}}_{new}(t) \sim \dot{\tilde{d}}(t)$ when time goes to infinity and Substituting Eq. (25) into Eq. (29) leads to

$$\dot{\tilde{d}}_{new}(t) = -\frac{\alpha}{\beta}\tilde{d}_{new}(t) \tag{30}$$

The chosen condition of α *and* β leads $\tilde{d}_{new}(t)$ and $\tilde{d}(t)$ to approach zero when time goes to infinity.

The disturbance gain L_d is selected by experience as long as the term $L_dG_3$in Eq. (26) is positively defined.

Remark 1: This article proposed the disturbance observer without knowledge of the disturbance information and its boundary. Therefore the disturbance with an unknown frequency will be completely estimated without the requirement of the first derivative of the disturbance value goes to zero when time going to infinity.

C. SYNCHRONIZATION OF TWO NON-IDENTICAL SYSTEMS BASED ON AN LMI CONTROL AND A DISTURBANCE OBSERVER

This section presents the synchronization method for two nonidentical models. Taking the derivative of both sides of Eq. (11) yields

$$\begin{aligned} \dot{e}(t) &= \dot{X}_m(t) - \dot{X}_s(t) \\ &= \sum_{i=1}^{r} \omega_{mi}(x_{1m}(t))\{(A_iX_m(t)) + E_{im}L_m(t)\} \\ &\quad - \sum_{i=1}^{r} \omega_{si}(x_{1s}(t))\{(A_iX_s(t)) + B_iu(t) + E_{is}L_s(t)\} \end{aligned} \tag{31}$$

Substituting $e(t) = X_m(t) - X_s(t)$ and $u_i(t) = K_{di}e(t)$ into Eq. (31) leads to

$$\begin{aligned}\dot{e}(t) &= \dot{X}_m(t) - \dot{X}_s(t)\\ &= \sum_{i=1}^{r} \omega_{mi}(x_{1m}(t))\{(A_iX_m(t)) + E_{im}L_m(t)\}\\ &\quad - \sum_{i=1}^{r} \omega_{si}(x_{1s}(t))\{(A_i(X_m(t) - e(t))) + B_iK_{di}e(t)\\ &\quad + E_{is}L_s(t)\}\end{aligned} \tag{32}$$

or

$$\begin{aligned}\dot{e}(t) &= \dot{X}_m(t) - \dot{X}_s(t)\\ &= \sum_{i=1}^{r} \omega_{mi}(x_{1m}(t))(A_iX_m(t))\\ &\quad - \sum_{i=1}^{r} \omega_{si}(x_{1s}(t))(A_i(X_m(t) - e(t)))\\ &\quad - \sum_{i=1}^{r} \omega_{si}(x_{1s}(t))B_iK_{di}e(t)\\ &\quad + \sum_{i=1}^{r} \omega_{mi}(x_{1m}(t))E_{im}L_m(t) - \sum_{i=1}^{r} \omega_{si}(x_{1s}(t))E_{is}L_s(t)\}\end{aligned} \tag{33}$$

Because $\sum_{i=1}^{r} \omega_{mi}(x_{1m}(t)) = 1$ and $\sum_{i=1}^{r} \omega_{si}(x_{1s}(t)) = 1$, Eq. (28) can be rewritten as

$$\begin{aligned}\dot{e}(t) &= \dot{X}_m(t) - \dot{X}_s(t)\\ &\quad \times \sum_{i=1}^{r} \omega_{si}(x_{1s}(t))[A_i - B_iK_{di}](e(t))\\ &\quad + \sum_{i=1}^{r} \omega_{mi}(x_{1m}(t))E_{im}L_m(t) - \sum_{i=1}^{r} \omega_{si}(x_{1s}(t))E_{is}L_s(t)\}\end{aligned} \tag{34}$$

For the system in Eq. (6), the term disturbance can be considered as the master system disturbance $E_mL_m(t)$ and the slave system disturbance is $E_sL_s(t)$. Then, Eq. (34) can be rewritten as

$$\begin{aligned}\dot{e}(t) &= \dot{X}_m(t) - \dot{X}_s(t)\\ &= \sum_{i=1}^{r} \omega_{si}(x_{1s}(t))[A_i - B_iK_{di}](e(t)) + E\bar{L}\end{aligned} \tag{35}$$

where $\bar{L}$ is the subtraction disturbance between the master and slave systems. By adding the estimated disturbance to the control input of the slave system, Eq. (35) could be rewritten as

$$\begin{aligned}\dot{e}(t) &= \dot{X}_m(t) - \dot{X}_s(t)\\ &= \sum_{i=1}^{r} \omega_{si}(x_{1s}(t))[A_i - B_iK_{di}]e(t)\\ &\quad - \sum_{i=1}^{r} \omega_{si}(x_{1s}(t))(E\hat{\bar{L}}_i - E\bar{L}_i)\end{aligned} \tag{36}$$

where $\sum_{i=1}^{r} \omega_{si}(x_{1s}(t)) = 1$. Again Eq. (36) can be rewritten as

$$\begin{aligned}\dot{e}(t) &= \dot{X}_m(t) - \dot{X}_s(t)\\ &= \sum_{i=1}^{r} \omega_{si}(x_{1s}(t))\{[A_i - B_iK_{di}]e(t) - E\tilde{\bar{L}}_i\}\end{aligned} \tag{37}$$

where $E\tilde{\bar{L}}_i = \sum_{i=1}^{r} \omega_{si}(x_{1s}(t))(E\hat{\bar{L}}_i - E\bar{L}_i)$. By applying the linear matrix inequality and disturbance observer, the derivative of the error approaches zero when time goes to infinity. The linear matrix inequality gain is determined by inserting the gain $A_i - B_iK_{di}$ into Eq. (18). The result is as follows:

$$\begin{cases}(A_i - B_iK_{di})P + P(A_i - B_iK_{di})^T + 2aP < 0\\ (A_i - B_iK_{di})P + P(A_i - B_iK_{di})^T + 2bP > 0\end{cases} \tag{38}$$

or

$$\begin{cases}A_iP + PA_i^T - B_iK_{di}P - PB_iK_{di}^T + 2aP < 0\\ A_iP + PA_i^T - B_iK_{di}P - PB_iK_{di}^T + 2bP > 0\end{cases} \tag{39}$$

The linear matrix gain is now defined as

$$K_{di} = -MP^{-1} \tag{40}$$

where $K_{di}P = M$.

Remark 2: The sum of the disturbance and uncertainty of the master and slave systems was considered by one term. This convention is a simple way to design a single disturbance with fully estimated effects of the disturbance and uncertainty on both systems.

IV. ILLUSTRATIVE EXAMPLES

This section presents two experimental studies of the proposed control synchronization method for the three-dimensional T-S fuzzy system in Eq. (6). Two case studies are given to show that the proposed synchronization control in this article is suitable for both secure communications of internet data and electronic circuit signal transmissions. This section confirms that the same function of communication can be achieved on electronic circuits.

There are two subsystems of the T-S fuzzy model of the 3-D chaotic system. The D-stability parameters are $r \to r_i$, $c \to c_i$, $a \to a_i$, and $b \to b_i$, furthermore, L_d, α, and β in Eq. (27) can be referred to L_{di}, α_i, and β_i, respectively. In Eq. (35) $E \to E_i$ and $\bar{L} \to \bar{L}_i$ where, $i = 1 \div 2$. Thus, the proposed control synchronization method can be applied to two subsystems together. The effective combination of the D-stability in the previous section, the disturbance observer in Eq. (27), and Eq. (35) for synchronizing the T-S fuzzy system are shown in two case studies.

A. SYNCHRONIZATION OF TWO COMPUTERS

The synchronization of two computers via an internet router is presented in this section. In this scenario the disturbance was selected as random values and formed as

$$d_{mi} = \begin{bmatrix}0\\ 0\\ d_{m3}(t)\end{bmatrix} \tag{41}$$

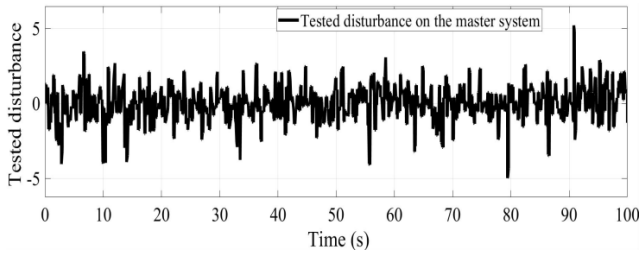

FIGURE 6. Tested disturbance value on the master system.

where the disturbance $d_{si} = 0$ and d_{m3} is shown in Figure 6 below.

The control parameters are $r_1 = 20$, $c_1 = 21$, $a_1 = 1$, $b_1 = 40$, and $r_2 = 15$, $c_1 = 20$, $a_2 = 6$, $b_1 = 34$ for the first and second subsystem error regions, respectively. The disturbance observer gains for these two regions are $L_{d1} = [0.1, 0.1, 50]$, and $L_{d2} = [0.1, 0.1, 25]$ respectively. The time-varying disturbance observer gains are $\alpha_1 = 50$, $\beta_1 = 10^{-4}$, and $\alpha_2 = 1.25$, $\beta_2 = 10^{-4}$.

Assumption 1: $x(t) \in [-5; 5]$ and the system parameters are $\omega_1(\theta(t)) = \frac{5+x(t)}{10}$ and $\omega_2(\theta(t) = \frac{5-x(t)}{10}$. The LMI gains are $K_{d1} = [9.0544, 7.5091, 17.3053]$,

$$K_{d2} = [132.6184, 21.8418, 11.7170].$$

$$A_1 = \begin{bmatrix} -1 & 2 & 0 \\ 0 & 0 & -5 \\ 5 & 5 & 0 \end{bmatrix}, \quad B_1 = \begin{bmatrix} 0 \\ 1 \\ 1 \end{bmatrix}, \quad E_1 = \begin{bmatrix} 1 \\ 1 \\ 1 \end{bmatrix},$$

$$A_2 = \begin{bmatrix} -1 & 2 & 0 \\ 0 & 0 & 5 \\ -5 & -5 & 0 \end{bmatrix}, \quad B_2 = \begin{bmatrix} 0 \\ 1 \\ 1 \end{bmatrix}, \quad E_2 = \begin{bmatrix} 1 \\ 1 \\ 1 \end{bmatrix} \text{ and}$$

$$C = [1 \quad 0 \quad 0].$$

The system error eigenvalues of $A_1 - B_1K_{d1}$ are $\lambda_{11} = -20.6337 + 0.0000i$, $\lambda_{12} = -2.5903 + 1.8159i$, and $\lambda_{13} = -2.5903 - 1.8159i$. The system error eigenvalues of the term $A_2 - B_2K_{d2}$ are $\lambda_{21} = -17.5772$, $\lambda_{22} = -8.4908 + 1.9586i$, and $\lambda_{23} = -8.4908 - 1.9586i$. The control synchronization setup is shown in Figure 7 below.

The computers' configurations are an Intel(R) Core(TM) i7-2600 CPU @ 3.40 GHz, RAM 4.00 GB and an Intel(R) Core(TM) i7-2600 CPU @ 3.40 GHz, RAM 10.0 GB for the master and slave systems, respectively. Both of these computers use Windows 10 64-bit. The given output signals of the synchronization for the computers are in Figure 8 below.

The received signals of the slave system are very close to the master system. The disturbance and uncertainty values affect the systems' output performance, and the system states will be changed definitely. This study used the time-varying disturbance observer to delete the disturbance and uncertainty of the transmission. The error signals of the transmission are now calculated from the sent and received system as shown in Fig. 9 below.

The transmission errors of two nonidentical T-S fuzzy systems are very small, and this feature was achieved by

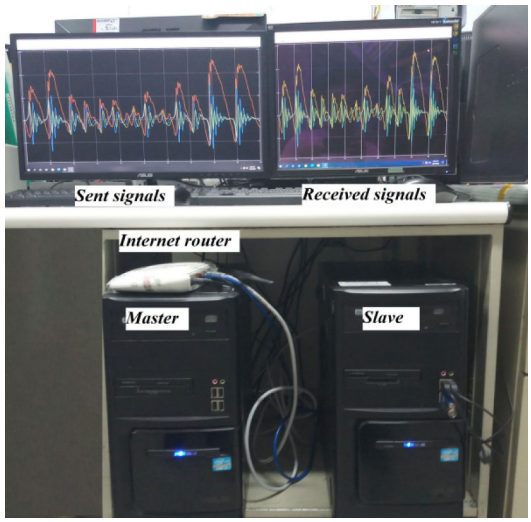

FIGURE 7. Two-computer synchronization setup system.

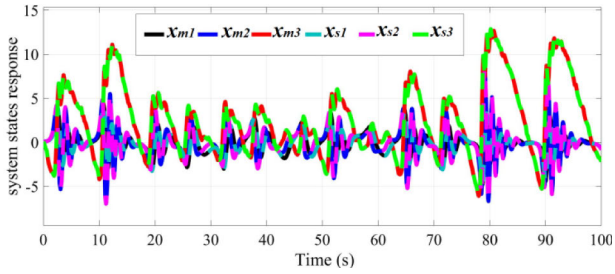

FIGURE 8. The response signals of the slave system and the transmitted signal of the master system.

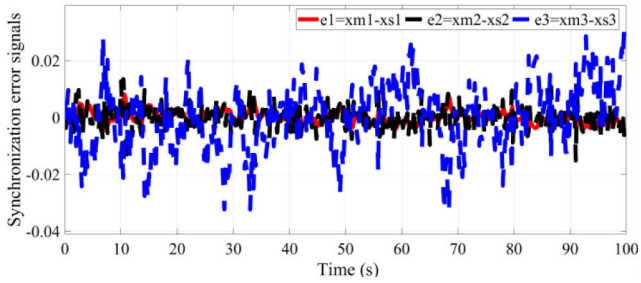

FIGURE 9. The error signals of the synchronization.

applying the time-varying disturbance observer to cancel the disturbance and uncertainty of the transmission process.

The slave output signals reached the master signal very quickly. Very few overshoot values appear in Figure 9a. In this case, the disturbance was tested by inserting it into the master system. The value of the tested disturbance can be seen in Figure 6 as a random signal that can easily be rejected by a new disturbance observer. The estimated disturbance and tested disturbance are shown in Figure 10 below.

The estimated disturbance and uncertainty values are marked by the red color in Figure 10 above. The tested disturbance is mostly rejected by compensating the disturbance

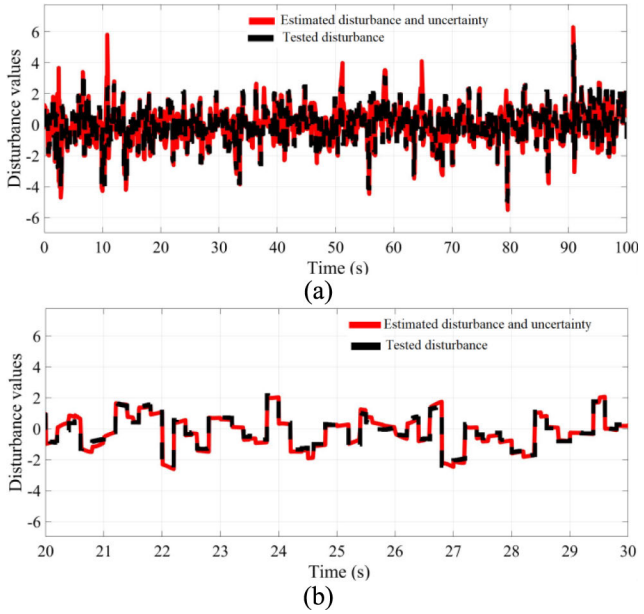

FIGURE 10. Disturbance and uncertainty estimation response signals of 100 seconds and a region of the signal consisting of 20 to 30 seconds: (a) tested disturbance in 100 seconds, (b) a region of the tested disturbance consisting of 20 to 30 seconds.

and uncertainty values, which implies that the output signals of the slave system closely tracked the master output signals.

B. SYNCHRONIZATION OF ELECTRONIC CIRCUITS

This section presents the synchronization of two electronic circuits that is based on the above theory. Due to the gains of the electronic circuits' limitation, this section selected the different gain values compared to the computers' communication in the previous section. The parameters of the control system are $r_1 = 5$, $c_1 = 10$, $a_1 = 1$, $b_1 = 9$, and $r_2 = 3$, $c_2 = 5$, $a_2 = 2$, $b_2 = 7$ for the first and second subsystem error regions, respectively. The disturbance observer gains are $L_{d1} = [0.1, 0.1, 5]$, and $L_{d2} = [0.1, 0.1, 10]$, respectively. The time-varying disturbance observer gains are $\alpha_1 = 24$, $\beta_1 = 0.1$, and $\alpha_2 = 49$, $\beta_2 = 0.1$.

Assumption 2: $x(\tau) \in [-5; 5]$, the system parameters are the same as the parameters in the previous part $\omega_1(\theta(t)) = \frac{5+x(t)}{10}$, $\omega_2(\theta(t)) = \frac{5-x(t)}{10}$, $A_1 = \begin{bmatrix} -1 & 2 & 0 \\ 0 & 0 & -5 \\ 5 & 5 & 0 \end{bmatrix}$, $B_1 = \begin{bmatrix} 0 \\ 1 \\ 1 \end{bmatrix}$, $E_1 = \begin{bmatrix} 1 \\ 1 \\ 1 \end{bmatrix}$, $A_2 = \begin{bmatrix} -1 & 2 & 0 \\ 0 & 0 & 5 \\ -5 & -5 & 0 \end{bmatrix}$, $B_2 = \begin{bmatrix} 0 \\ 1 \\ 1 \end{bmatrix}$, $E_2 = \begin{bmatrix} 1 \\ 1 \\ 1 \end{bmatrix}$ and $C = [1 \ 0 \ 0]$.

The LMI gains are

$K_{d1} = [-0.8629, -2.0154, 22.7895]$ and $K_{d2} = [2.2202, 5.3071, 4.7628]$. The system error eigenvalues of $A_1 - B_1K_{d1}$ are $\lambda_{11} = -5.6874$, $\lambda_{12} = -8.0433 + 3.4475i$, and $\lambda_{13} = -8.0433 - 3.4475i$. The system error eigenvalues of the term $A_2 - B_2K_{d2}$ are $\lambda_{21} = -2.5510$, $\lambda_{22} = -4.2594 + 1.5354i$, and $\lambda_{23} = -4.2594 - 1.5354i$. The simulation of two nonidentical synchronizations is in the appendix's Figs. 1-3. The simulation results are shown in Figure 11.

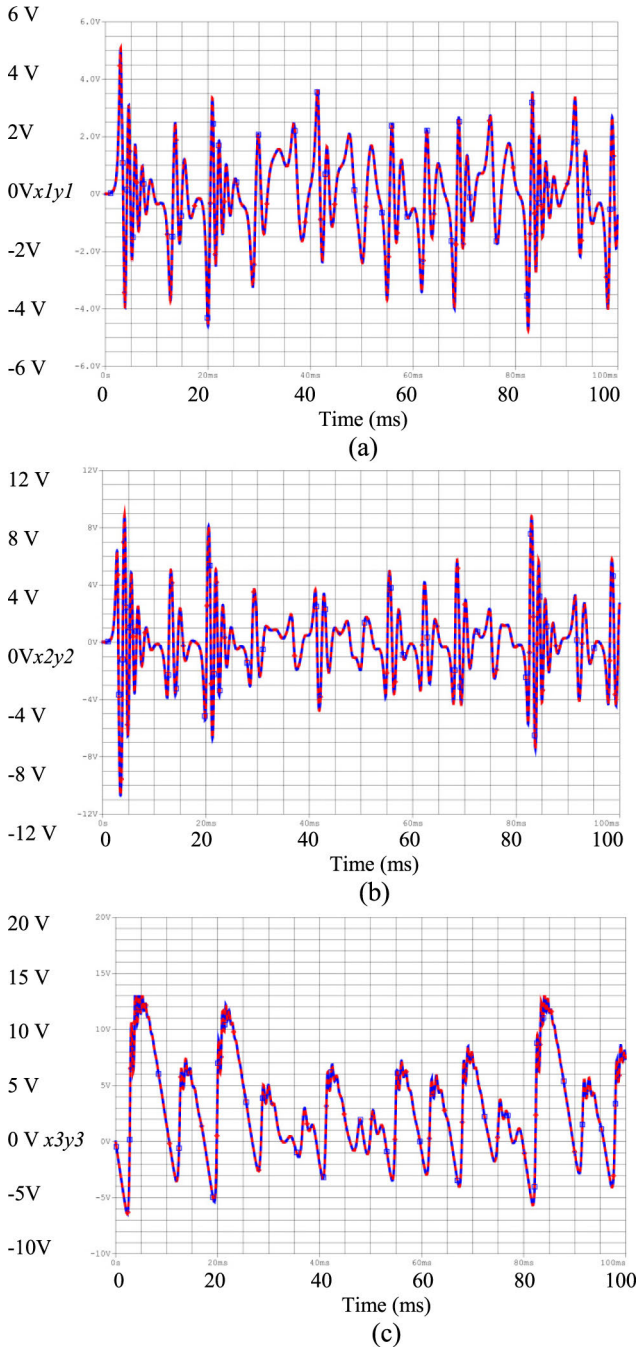

FIGURE 11. Two electronic circuits' synchronization simulation results: (a) *x1* and *y1* trajectories, (a) *x2* and *y2* trajectories, (a) *x3* and *y3* trajectories.

The blue color is used to represent the master signal, and the red color corresponds to the slave signal. The simulation of electronic circuit synchronization achieved a good result with very small tracking error values and small overshoots. Furthermore, the responses of the slave to the master system are very rapid. This simulation is obtained on millisecond

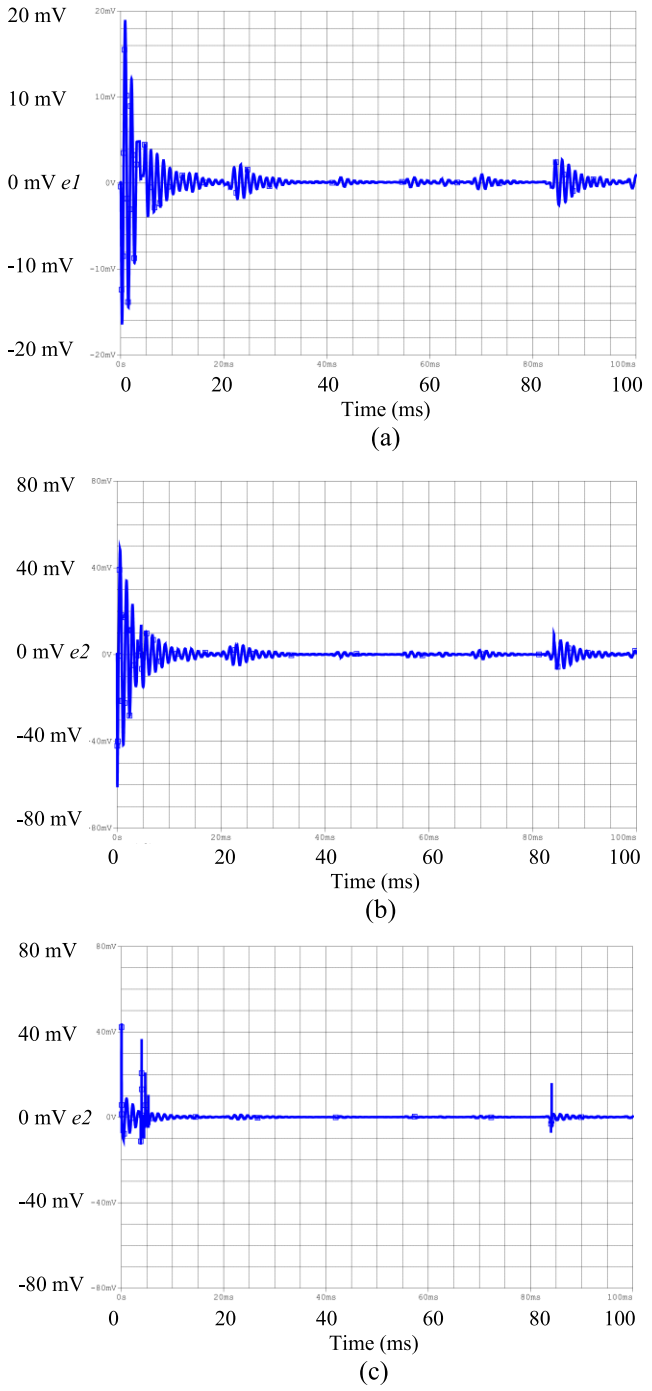

FIGURE 12. Tracking error values: (a) e1 signal, (b) e2 signal, (c) e3 signal.

scales, which is meant to aid a decision on selecting the electronic components. The tracking error values are calculated in Figure 12 below. The tracking error values are calculated in Figure. 12 below.

The given output of the simulation in Orcad Capture software was shown with small tracking error values. The errors of the x-state, y-state, and z-state range from $[-16$ mV, 19 mV$]$, $[-60$ mV, 50 mV$]$, and $[-12$ mV, 42 mV$]$, respectively. The system states of the master and slave are very close to each other, and they are used to confirm that the proposed

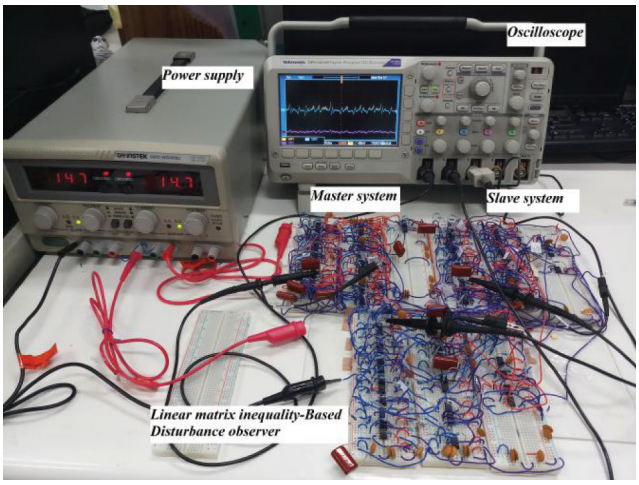

FIGURE 13. A synchronization setup system with two electronic circuits.

control method is effective at the synchronization of two nonidentical T-S fuzzy 3-D chaotic systems. The control system was constructed by means of the circuits in Figure 13 below.

The experiments' electrical voltage was supplied by the Laboratory DC power supply through a GWINSTEK GPC-6030-D Dual tracking with a machine fixed at 5 V. The performance of the system was displayed by the Tektronix DPO 2014B digital phosphor oscilloscope. The Takagi-Sugeno fuzzy system phase portraits are shown in Figure 14 below.

The real circuit phase portraits are quite similar to the simulation phase portraits of the MATLAB simulation and the Orcard Capture simulation. In terms of the constant value d, the third equation in Eq. (1) determines the phase portraits definitively. The given phase portraits of the experiment on the electronic circuit again confirm that the proposed model can be completely converted to the Takagi-Sugeno fuzzy mode on a milliseconds time scale. Conversion of the system mode still retains the original conservative characteristics of the 3-D chaotic system. This article used the linear matrix inequality to obtain the control gains, and it used the disturbance observer to delete unwanted value values from the system. The implementation results of the real circuits are shown in Figure 15 below.

The disturbance of the electronic main boards along with the resistors and capacitors changing the temperature, which mostly compensated the slave system like the estimated disturbance and uncertainty in Figure 16 below.

The synchronization of two nonidentical T-S fuzzy systems was implemented on the electronic circuit perfectly. The slave system states are closed to the master system states, and the tracking error is very small. The estimated disturbance and uncertainty are given as the value of the electronic board resister and the capacitor values. The errors of the master and slave system states are $e1 = [-0.6\text{ V}, 0.2\text{ V}]$, $e2 = [-0.45\text{ V}, 0.6\text{ V}]$, and $e3 = [-0.1\text{ V}, 0.6\text{ V}]$. The time-varying disturbance observer and D-stability are correctly applied to the synchronization of the 3-D T-S fuzzy chaotic system. Two illustrative examples are included.

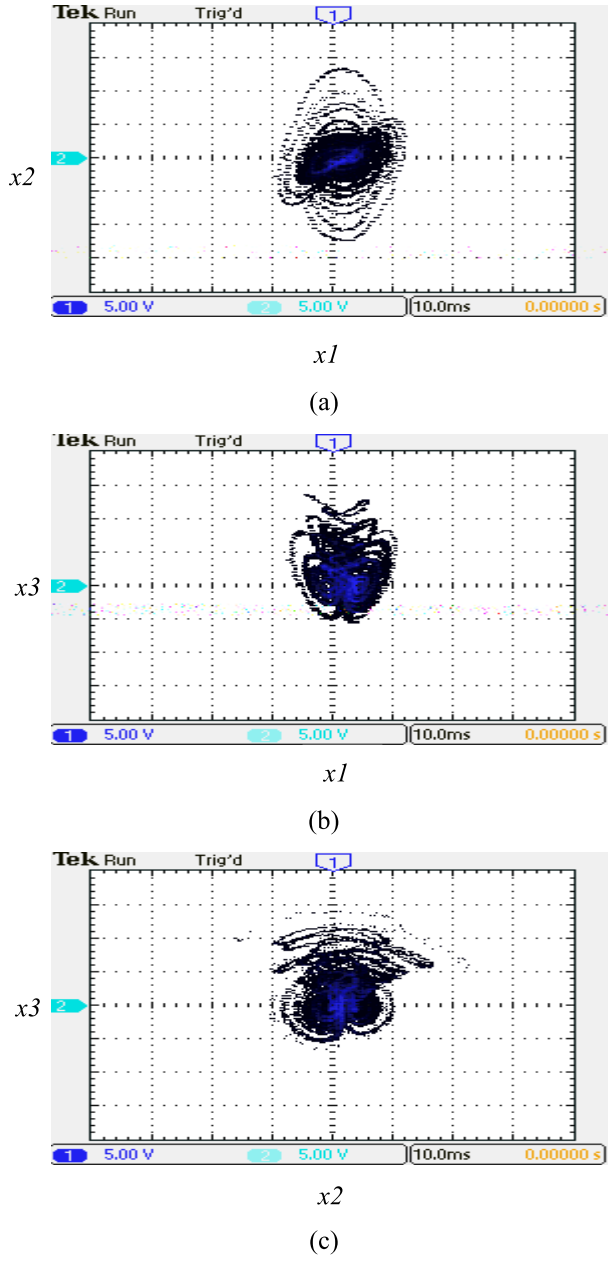

FIGURE 14. System phase portraits: (a) x2-x1 phase portrait, (b) x3-x1 phase portrait, (c) x3-x2 phase portrait.

TABLE 1. Comparison of synchronization states' error maximum values.

Value	Our paper results	Paper [3] results
Overshoot	Mostly equal to zero	0.5
Range of state's error	[-0.03;0.03]	[-0.2;0.5]
Settling time	Mostly equal to zero	After 5 seconds
Background	Experiment	Simulation

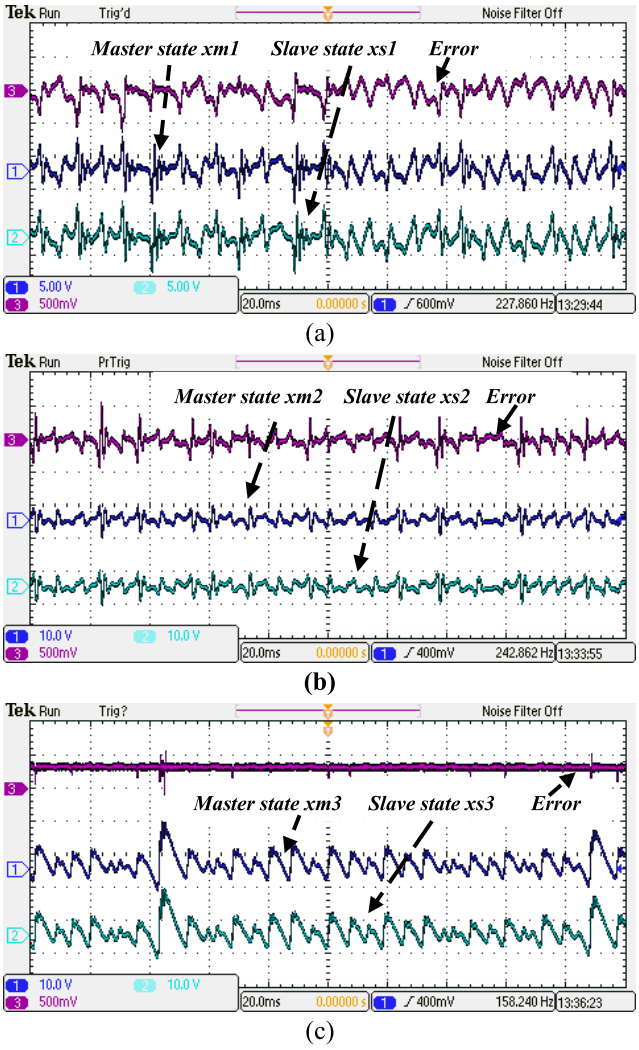

FIGURE 15. Two electronic circuits' synchronization given output: (a) xm1 and xs2 signals, (b) xm2 and xs2 signals, (c) xm3 and xs3 signals.

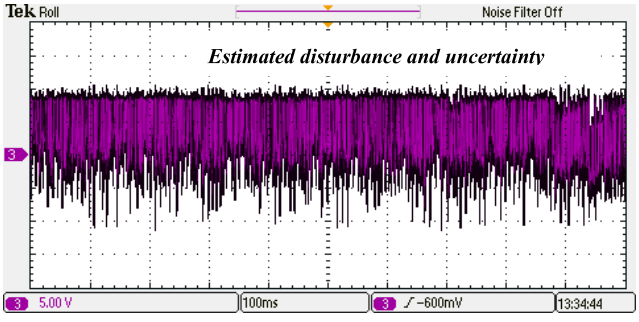

FIGURE 16. Estimated disturbance and uncertainty values of two electronic circuits' synchronization.

No prior paper deals with synchronization of the 3-D chaotic model in Eq. (1) and with the method for synchronization as the combination of D-stability and a new disturbance observer. This comparison affirms that the proposed control synchronization of this study can obtain a very good transient response with very little overshooting and with stability. The comparison is given in Table 1 below.

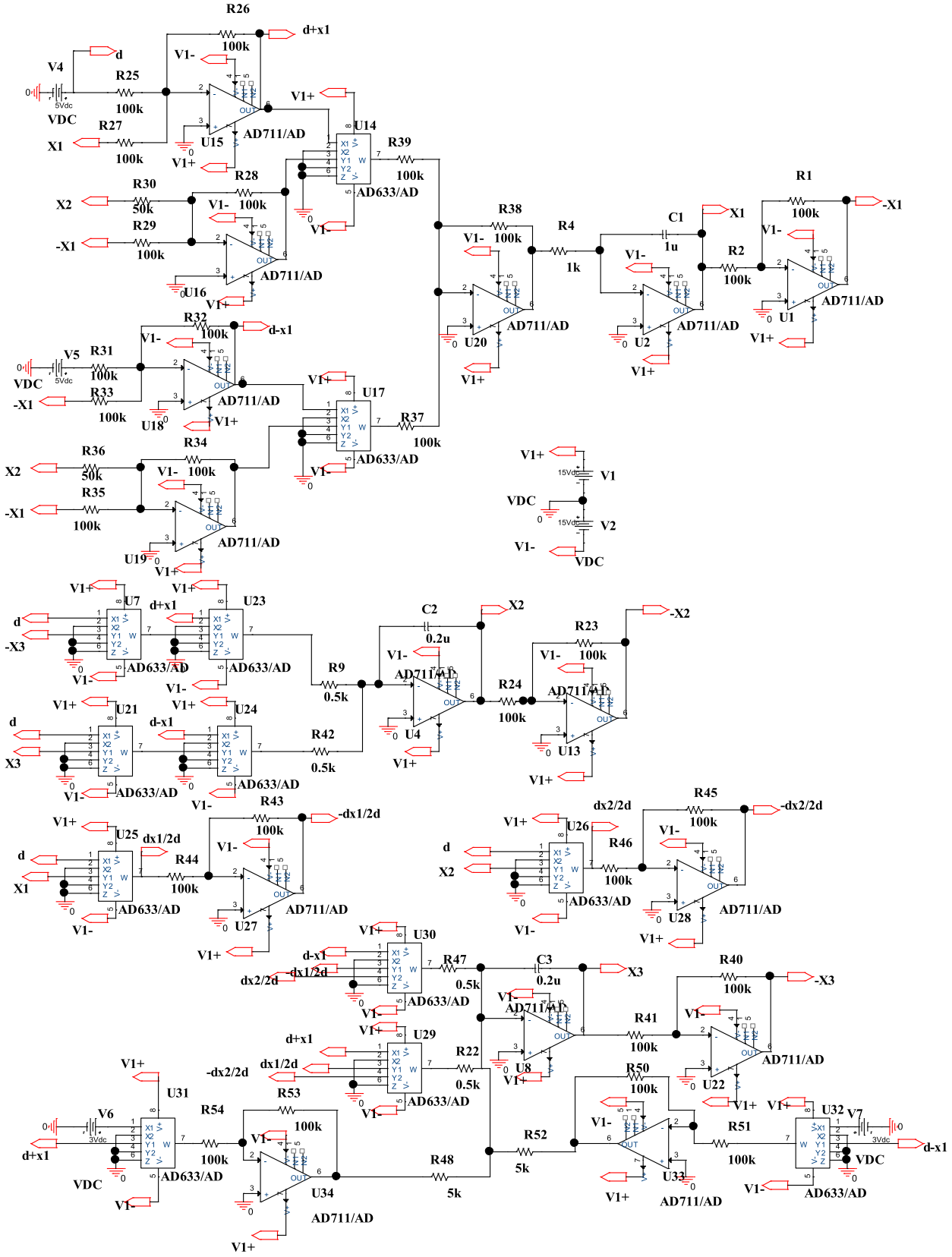

FIGURE 17. Master system in electronic circuit modeling.

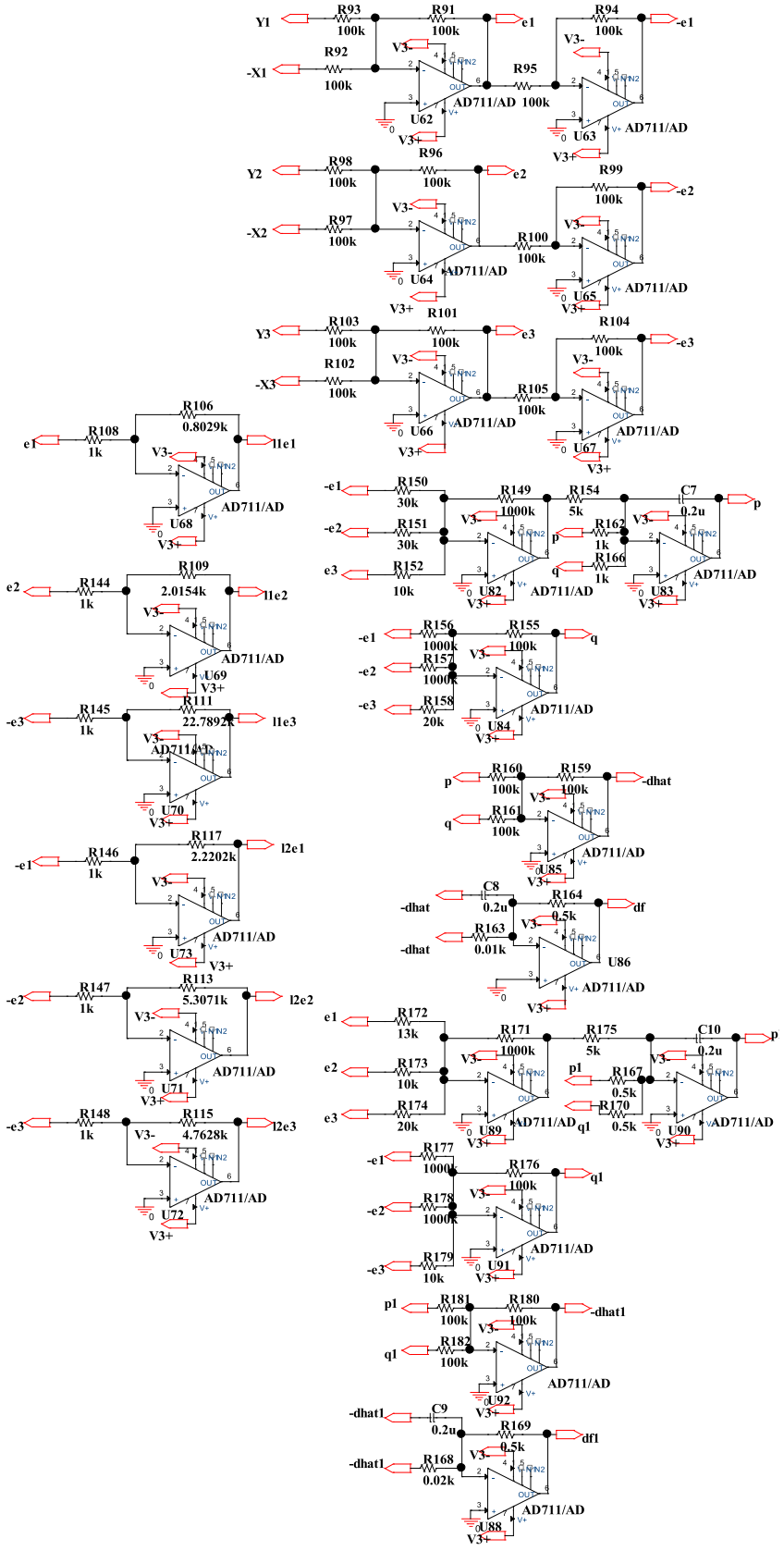

FIGURE 18. Linear matrix inequality and disturbance observer modeling in electronic circuit.

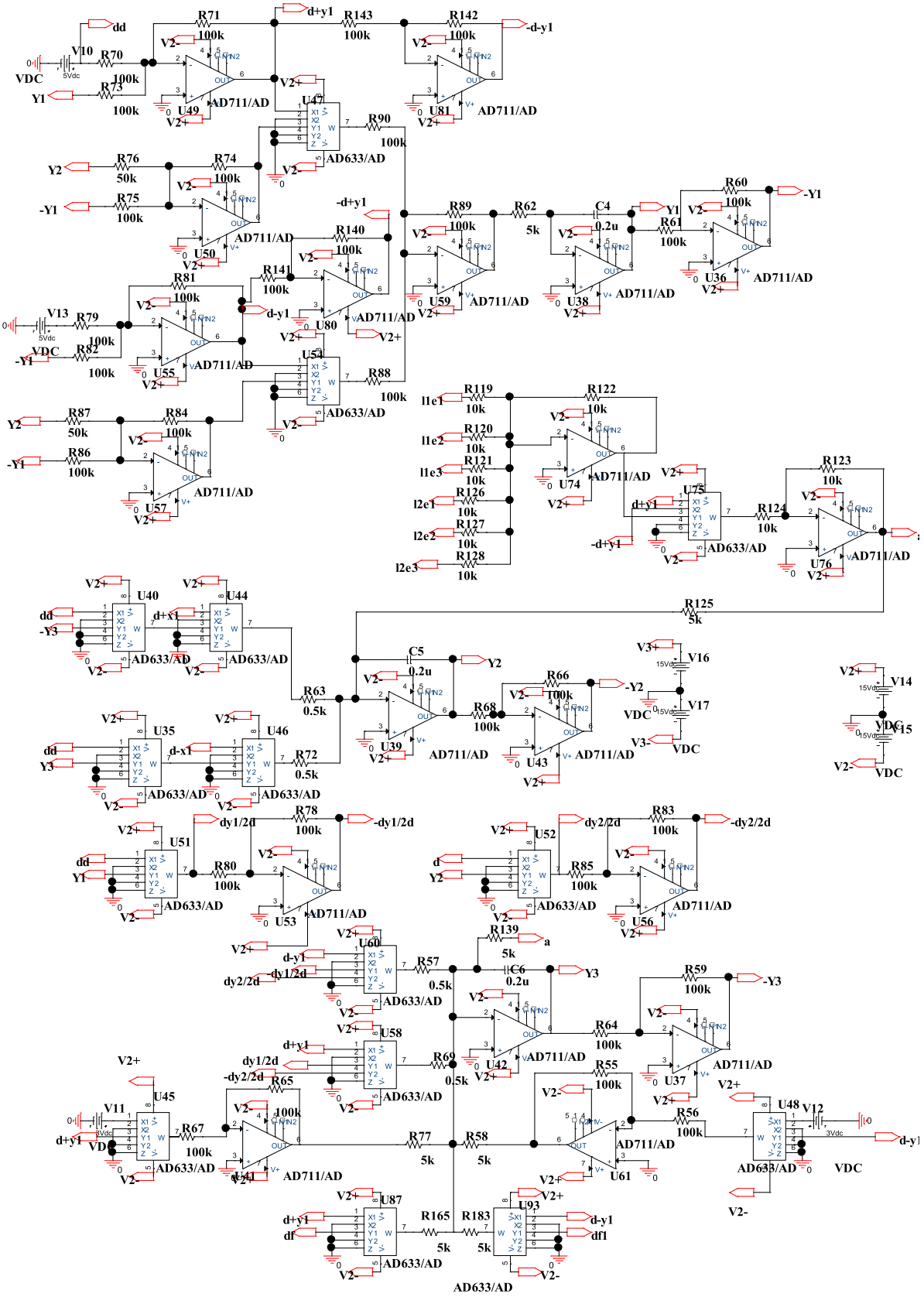

FIGURE 19. Slave system in electronic circuit modeling.

V. CONCLUSION

This article presented the control synchronization of two nonidentical chaotic systems, which were converted to a new form of the T-S fuzzy system. The control synchronization was based on the linear matrix inequality convex optimization method and a time-varying disturbance observer. The linear matrix inequality was applied to determine the eigenvalues of the error states. The system error eigenvalues were located in the convex optimized area. The author' ideas were perfectly achieved by the computers' communication via a local network router, and the electronic circuits' communication. The given outputs of the slave system states are closed to the sent signals of the master system. Furthermore, the disturbance and uncertainty were mostly suppressed, and they were used to confirm that the proposed control algorithm is ideal for the synchronization of two nonidentical chaotic systems. The cost of the experiment of the electronic circuit synchronization was cheaper than the cost of the computer synchronization. This work gives a suggestion for our future works in secure communications, which will be based on electronic circuits.

APPENDIX

This section used X for *xm* and Y for *xs*, df for $L_1(t)$ and df1 for $L_2(t)$. The master, slave, and control systems are shown in the Appendix figures below.

See Figs. 17–19.

REFERENCES

[1] Z. Hua, Y. Zhang, and Y. Zhou, "Two-dimensional modular chaotification system for improving chaos complexity," *IEEE Trans. Signal Process.*, vol. 68, pp. 1937–1949, 2020.
[2] Y. Huang, L. Huang, Y. Wang, Y. Peng, and F. Yu, "Shape synchronization in driver-response of 4-D chaotic system and its application in image encryption," *IEEE Access*, vol. 8, pp. 135308–135319, 2020.
[3] S. Mobayen and F. Tchier, "Synchronization of a class of uncertain chaotic systems with Lipschitz nonlinearities using state-feedback control design: A matrix inequality approach," *Asian J. Control*, vol. 20, no. 1, pp. 71–85, Jan. 2018.
[4] L. Zhou and F. Tan, "A chaotic secure communication scheme based on synchronization of double-layered and multiple complex networks," *Nonlinear Dyn.*, vol. 96, no. 2, pp. 869–883, Apr. 2019.
[5] L. Zhou, F. Tan, F. Yu, and W. Liu, "Cluster synchronization of two-layer nonlinearly coupled multiplex networks with multi-links and time-delays," *Neurocomputing*, vol. 359, pp. 264–275, Sep. 2019.
[6] H. Lin, C. Wang, and Y. Tan, "Hidden extreme multistability with hyper-chaos and transient chaos in a hopfield neural network affected by electromagnetic radiation," *Nonlinear Dyn.*, vol. 99, no. 3, pp. 2369–2386, Feb. 2020.
[7] A. D. Pano-Azucena, J. de Jesus Rangel-Magdaleno, E. Tlelo-Cuautle, and A. de Jesus Quintas-Valles, "Arduino-based chaotic secure communication system using multi-directional multi-scroll chaotic oscillators," *Nonlinear Dyn.*, vol. 87, no. 4, pp. 2203–2217, Mar. 2017.
[8] G. Wen, Y. Wan, J. Cao, T. Huang, and W. Yu, "Master–Slave synchronization of heterogeneous systems under scheduling communication," *IEEE Trans. Syst., Man, Cybern. Syst.*, vol. 48, no. 3, pp. 473–484, Mar. 2018.
[9] T. Wang, D. Wang, and K. Wu, "Chaotic adaptive synchronization control and application in chaotic secure communication for industrial Internet of Things," *IEEE Access*, vol. 6, pp. 8584–8590, 2018.
[10] H. Liu, Y. Zhang, A. Kadir, and Y. Xu, "Image encryption using complex hyper chaotic system by injecting impulse into parameters," *Appl. Math. Comput.*, vol. 360, pp. 83–93, Nov. 2019.
[11] J. Wang, J. Li, X. Di, J. Zhou, and Z. Man, "Image encryption algorithm based on bit-level permutation and dynamic overlap diffusion," *IEEE Access*, vol. 8, pp. 160004–160024, 2020.
[12] F. Yang, J. Mou, K. Sun, Y. Cao, and J. Jin, "Color image compression-encryption algorithm based on fractional-order memristor chaotic circuit," *IEEE Access*, vol. 7, pp. 58751–58763, 2019.
[13] C. S. Pappu, B. C. Flores, P. S. Debroux, and J. E. Boehm, "An electronic implementation of lorenz chaotic oscillator synchronization for bistatic radar applications," *IEEE Trans. Aerosp. Electron. Syst.*, vol. 53, no. 4, pp. 2001–2013, Aug. 2017.
[14] S. Yang, C. Li, and T. Huang, "Synchronization of coupled memristive chaotic circuits via state-dependent impulsive control," *Nonlinear Dyn.*, vol. 88, no. 1, pp. 115–129, Apr. 2017.
[15] M. Kountchou, P. Louodop, S. Bowong, H. Fotsin, and Saïdou, "Analog circuit design and optimal synchronization of a modified Rayleigh system," *Nonlinear Dyn.*, vol. 85, no. 1, pp. 399–414, Jul. 2016.
[16] C. Li, F. Min, and C. Li, "Multiple coexisting attractors of the serial–parallel memristor-based chaotic system and its adaptive generalized synchronization," *Nonlinear Dyn.*, vol. 94, no. 4, pp. 2785–2806, Dec. 2018.
[17] Y.-J. Chen, H.-G. Chou, W.-J. Wang, S.-H. Tsai, K. Tanaka, H. O. Wang, and K.-C. Wang, "A polynomial-fuzzy-model-based synchronization methodology for the multi-scroll chen chaotic secure communication system," *Eng. Appl. Artif. Intell.*, vol. 87, Jan. 2020, Art. no. 103251.
[18] T. Takagi and M. Sugeno, "Fuzzy identification of systems and its applications to modeling and control," *IEEE Trans. Syst., Man, Cybern.*, vol. SMC-15, no. 1, pp. 116–132, Jan. 1985.
[19] K. Tanaka and H. Wang, *Fuzzy Control Systems Design and Analysis: A Linear Matrix Inequality Approach*. New York, NY, USA: Wiley, 2001.
[20] G. Feng, "A survey on analysis and design of model-based fuzzy control systems," *IEEE Trans. Fuzzy Syst.*, vol. 14, no. 5, pp. 676–697, Oct. 2006.
[21] S. H. Tsai and Y. W. Chen, "A novel identification method for Takagi–Sugeno fuzzy model," *Fuzzy Sets. Syst.*, vol. 338, 117-135, 2018.
[22] A. Cherifi, K. Guelton, and L. Arcese, "Uncertain T-S model-based robust controller design withD-stability constraints—A simulation study of quadrotor attitude stabilization," *Eng. Appl. Artif. Intell.*, vol. 67, pp. 419–429, Jan. 2018.
[23] H. K. Lam, "A review on stability analysis of continuous-time fuzzy-model-based control systems: From membership-function-independent to membership-function-dependent analysis," *Eng. Appl. Artif. Intell.*, vol. 67, pp. 390–408, Jan. 2018.
[24] V.-P. Vu, W.-J. Wang, H.-C. Chen, and J. M. Zurada, "Unknown input-based observer synthesis for a polynomial T–S fuzzy model system with uncertainties," *IEEE Trans. Fuzzy Syst.*, vol. 26, no. 3, pp. 1447–1458, Jun. 2018.
[25] R. Sakthivel, K. Raajananthini, O. M. Kwon, and S. Mohanapriya, "Estimation and disturbance rejection performance for fractional order fuzzy systems," *ISA Trans.*, vol. 92, pp. 65–74, Sep. 2019.
[26] R. Sakthivel, S. Harshavarthini, R. Kavikumar, and Y.-K. Ma, "Robust tracking control for fuzzy Markovian jump systems with time-varying delay and disturbances," *IEEE Access*, vol. 6, pp. 66861–66869, 2018.
[27] P. Selvaraj, R. Sakthivel, and H. R. Karimi, "Equivalent-input-disturbance-based repetitive tracking control for Takagi–Sugeno fuzzy systems with saturating actuator," *IET Control Theory Appl.*, vol. 10, no. 15, pp. 1916–1927, Oct. 2016.
[28] J. H. Kim, C. H. Hyun, E. Kim, and M. Park, "Adaptive synchronization of uncertain chaotic systems based on T–S fuzzy model," *IEEE Trans. Fuzzy Syst.*, vol. 15, no. 3, pp. 359–369, Jun. 2007.
[29] H. S. Kim, J. B. Park, and Y. H. Joo, "Fuzzy-model-based sampled-data chaotic synchronisation under the input constraints consideration," *IET Control Theory Appl.*, vol. 13, no. 2, pp. 288–296, Jan. 2019.
[30] H. K. Lam, W. K. Ling, H. H. Iu, and S. S. Ling, "Synchronization of chaotic systems using time-delayed fuzzy state-feedback controller," *IEEE Trans. Circuits Syst. I, Reg. Papers*, vol. 55, no. 3, pp. 893–903, May 2008.
[31] Y. Zhao, B. Li, J. Qin, H. Gao, and H. R. Karimi, "H_∞ consensus and synchronization of nonlinear systems based on a novel fuzzy model," *IEEE Trans. Cybern.*, vol. 43, no. 6, pp. 2157–2169, Dec. 2013.
[32] R. Wang, B. Li, Z. Zhao, J. Guo, and Z. Zhu, "Synchronization of fuzzy control design based on bessel–legendre inequality for coronary artery state time-delay system," *IEEE Access*, vol. 7, pp. 1941–181933, 2019.
[33] R. Sakthivel, R. Sakthivel, O.-M. Kwon, and P. Selvaraj, "Synchronisation of stochastic T–S fuzzy multi-weighted complex dynamical networks with actuator fault and input saturation," *IET Control Theory Appl.*, vol. 14, no. 14, pp. 1957–1967, Sep. 2020.
[34] Z. Lendek, T. Guerra, R. Babuska, and B. D. Schutter, *Stability Analysis and Nonlinear Observer Design Using Takagi–Sugeno Fuzzy Models*. Dordrecht, The Netherlands: Springer-Verlag, 2010.

[35] J. Liu, Q. Qu, and G. Li, "A new six-term 3-D chaotic system with fan-shaped Poincaré maps," *Nonlinear Dyn.*, vol. 82, no. 4, pp. 2069–2079, Dec. 2015.
[36] W.-H. Chen, "Disturbance observer based control for nonlinear systems," *IEEE/ASME Trans. Mechatronics*, vol. 9, no. 4, pp. 706–710, Dec. 2004.
[37] M. Chilali, P. Gahinet, and P. Apkarian, "Robust pole placement in LMI regions," *IEEE Trans. Autom. Control*, vol. 44, no. 12, pp. 2257–2270, Dec. 1999.
[38] C. Mahmoud and G. Pascal, "H_∞ design with pole placement constraints: An LMI approach," *IEEE Trans. Autom. Control*, vol. 41, no. 3, pp. 67–358, Mar. 1996.
[39] D. Henrion, Q. Bachelier, and M. Sebek, "*D*-stability of polynomial matrices," *Int. J. Control*, vol. 8, no. 8, pp. 845–856, Nov. 2001.

VAN NAM GIAP received the B.S. degree in control engineering and automation from the Ha Noi University of Science and Technology, Hanoi, Vietnam, in 2015, and the master's degree in electronic engineering from the National Kaohsiung University of Applied and Sciences, Kaohsiung, Taiwan, in 2017. He is currently pursuing the Ph.D. degree in mechanical engineering with the National Kaohsiung University of Science and Technology, Taiwan, R.O.C. His research interests include sliding mode control, disturbance and uncertainty estimation, fuzzy logic control, and the magnetic bearing systems and its applications.

SHYH-CHOUR HUANG (Senior Member, IEEE) received the bachelor's degree in aeronautics and astronautics engineering from National Cheng Kung University, Taiwan, R.O.C., in 1980, and the Ph.D. degree in mechanical engineering from the University of Cincinnati, USA, in 1990. He is currently a Professor of mechanical engineering with the National Kaohsiung University of Science and Technology, Taiwan, R.O.C. His research interests include micro-electromechanical systems' design, biomechanics, compliant mechanisms, multibody dynamics, fuzzy logic control, vibration control, and optimization algorithms.

QUANG DICH NGUYEN received the B.S. degree in electrical engineering from the Hanoi University of Technology, Hanoi, Vietnam, in 1997, the M.S. degree in electrical engineering from the Dresden University of Technology, Dresden, Germany, in 2003, and the Ph.D. degree from Ritsumeikan University, Kusatsu, Japan, in 2010. Since 2000, he has been with the Hanoi University of Science and Technology, Vietnam, where he is currently an Associate Professor and the Executive Dean of the Institute for Control Engineering and Automation. His research interests include magnetic bearings, self-bearing motors, and sensorless motor control.

TE-JEN SU (Senior Member, IEEE) received the Ph.D. degree in electrical engineering from National Cheng Kung University, Tainan, Taiwan, in 1989. He is currently a Professor with the Department of Electronic Engineering, National Kaohsiung University of Science and Technology, Kaohsiung, Taiwan. His research interests include intelligent control systems, embedded processor designs, and satellite communication systems.